WPMAT-PR(18) 21510

C Robertson et al.

Screw dislocation interaction with irradiation defect-loops in alpha-iron: evaluation of loop-induced stress field effect using dislocation dynamics simulations

Preprint of Paper to be submitted for publication in
Nuclear Instruments and Methods in Physics Research
Section B

This work has been carried out within the framework of the EUROfusion Consortium and has received funding from the Euratom research and training programme 2014-2018 under grant agreement No 633053. The views and opinions expressed herein do not necessarily reflect those of the European Commission.

Screw dislocation interaction with irradiation defect-loops in α-iron: evaluation of loop-induced stress field effect using dislocation dynamics simulations

Y. Li*, C. Robertson, M. Shukeir, L. Dupuy

DEN-Service de Recherches Métallurgiques Appliquées, CEA, Université Paris-Saclay, F-91191, Gif-sur-Yvette, France

Abstract

Plastic strain spreading in post-irradiated Fe grains takes the form of wavy shear bands, where mobile dislocations interact with the radiation defect dispersions. In actual Fe grains, dislocation/loop interactions involve several contributing factors including: screw dislocation cross-slip and loop-induced stress. The loop-induced stress effect is here evaluated by systematic simulation case comparisons, using adapted dislocation dynamics simulations. Namely, dislocation/loop simulation cases are systematically compared with equivalent dislocation/facet simulation cases, under room temperature straining conditions. The facets have exactly the same size and orientation as in the reference loop cases, however; the facets have no associated stress field. It is thereby found that in presence of cross-slip the total reaction time and reaction strain associated with various dislocation/facet cases is close to their dislocation/loop counterparts (within 15% and 12%, respectively). In the present investigation context, loop-induced stress field contribution is thus a second order effect, regardless of the considered loop type and orientation. In this situation, the calculation-intensive dislocation/loop interaction description can be replaced by the much faster dislocation/facet approach, for computationally intensive grain-scale simulations.

Keywords: cross slip effect; radiation-induced defects; loop-induced stress field; dislocation dynamics simulation

* Corresponding author
Email address: yang.li@cea.fr (Y. Li).

1. Introduction

Ferritic α-iron steels are widely used as pressure vessel materials, in Pressurized Water nuclear Reactors (PWR). Exposure to neutron irradiation causes detrimental degradation of the steel mechanical properties, including hardening and embrittlement [1]-[3]. These evolutions are generally ascribed to the gradual accumulation of dispersed defect cluster populations, mainly in the form of dislocation loops [4]-[5]. At the Fe grain scale, plastic strain spreading takes the form of wavy shear bands, where mobile dislocations strongly interact with dislocation loops [6]-[8], thereby affecting the subsequent stress-strain and fracture toughness responses [9]-[10].

In the past few years, dislocation/loop interaction mechanisms have been investigated using atomistic Molecular Dynamics (MD) [11]-[12] and mesoscopic Dislocation Dynamics (DD) simulations [13]-[14]. The influence of cross-slip on dislocation/loop interaction has recently been addressed by taking advantage of particular (see Fig. 1), three-dimensional nodal DD simulation setups [15]-[14]. The present work aims at evaluating the specific contribution of the loop-induced stress field on dislocation/loop interaction with respect to dislocation mobility, in presence of cross-slip mechanism and under room temperature straining conditions. This effect is highlighted by systematic comparison between simulation setups where the loops have been replaced by hard impenetrable platelets (or facets), without any associated elastic stress field.

The paper is organized as follows: the simulation model, setups and material parameters are presented in Section 2.1. The specific «composite» source configuration, adapted to cross-slip mechanism investigation, is described in Section 2.2 and further analyzed in Section 2.3. Benchmarking case of the infinite-long screw dislocation interaction with obstacles is presented in Section 3.1. Interactions of composite source with $[1\bar{1}1]$ and [111] facets are examined and then compared with the dislocation/loop cases, in Sections 3.2 and 3.3 respectively. The contribution of the elastic stress field and differences between loop and facet cases are further discussed in Section 3.4. This paper focuses on pure Fe, for which all the material parameters are well-characterized [13],[17]-[18].

2. Simulation method and setups

2.1 Dislocation Dynamics simulation setup

All DD simulations results presented in this work are performed using a 3D nodal code called NUMODIS (e.g. [13]-[14]), developed in CEA/SRMA (France). The dislocation lines are described by a series of inter-connected nodes. Computation of the internal elastic stress and the corresponding nodal force is carried out within the frame of the non-singular continuum elastic theory [19]. The stress at any arbitrary point is due to the total stress field:

$$\sigma = \sigma^{app} + \sigma^{int} \quad (1)$$

including the applied σ^{app} and internal σ^{int} stress field contributions. The force per unit length on the connected dislocation nodes is given by Peach-Koehler formula:

$$\mathbf{f}^{PK} = (\sigma \cdot b) \times \xi \quad (2)$$

where ξ is the local line direction, and b is the dislocation Burgers vector. The PK force, together with the contribution associated with the dislocation core energy is converted into nodal force by a weighting shape function. The present study is restricted to room temperature straining conditions, where screw dislocation velocity is a quasi linear function of the effective shear stress, through an effective drag coefficient B [17]-[18],[20]. The material parameters corresponding to pure Fe grains are listed in Tab. 1 below.

Viscous drag coefficient B (10^{-5} Pa s)	**Burgers vector b(10^{-10} m)**	**Shear modulus μ (GPa)**	**Poisson ration ν**	**Primary slip system**	**Cross-slip system**
8	2.54	62.9	0.43	$(1\bar{1}0)[111]$	$(10\bar{1})[111]$

Tab. 1. Pure Fe materials parameters at 300K [13],[17]-[18].

Our DD simulation results are first benchmarked by comparison with MD simulations using exactly the same configuration as shown in Fig. 1(a) [11]. The simulated crystal orientations as X, Y and Z axis are drawn parallel to the $[\bar{1}\bar{1}2]$, $[1\bar{1}0]$ and $[111]$ directions, respectively. The DD simulated volume dimensions are: L_X = 400 nm, L_Y = 300 nm and L_Z = 300 nm, which is comparable to the shear band thickness observed in post-irradiated, strained materials [10],[21]. Periodic boundary conditions are applied in X and Z directions. An infinite long screw dislocation line with Burgers vector ***b*** parallel to the Z direction is placed in the highlighted glide plane. One hexagonally shaped interstitial loop or impenetrable facet (platelet) is placed at a short initial distance from the mobile dislocation line. The facet has exactly the same size (D = 6 nm) and orientation $[1\bar{1}1]$ or [111] as the reference loop case. It is recalled that unlike the interacting dislocation loops, the implemented facets have strictly no associated stress field.

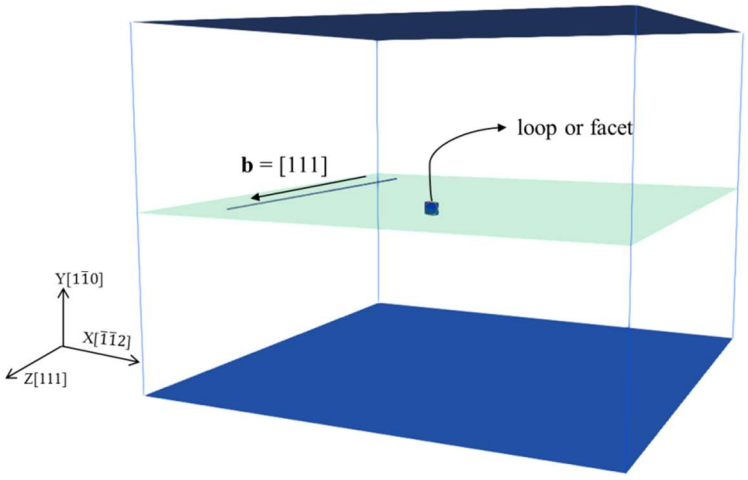

(a)

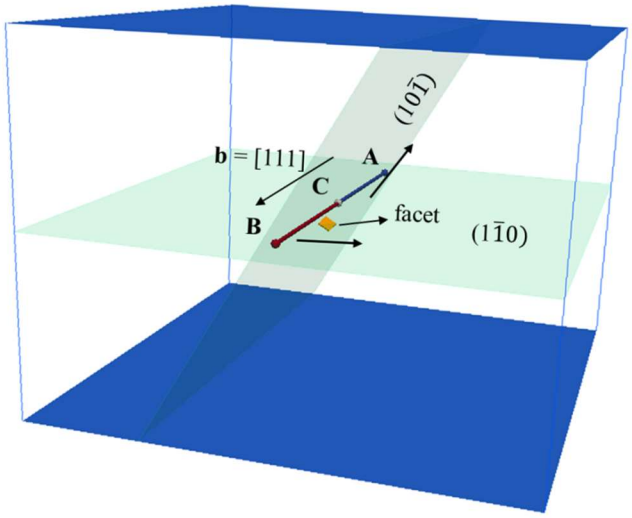

(b)

Fig. 1. Simulation volume configurations. (a) Benchmarking case. The highlighted primary slip plane contains an infinite screw dislocation and a dislocation loop (or a facet). (b) Composite dislocation source configuration with fixed nodes A and B. Segment AC is L_{cs} long and glides in the cross-slip plane $(10\bar{1})$; segment BC is L_p long and glides in the primary slip plane $(1\bar{1}0)$. Finite length sources are compatible with TEM observation of post-irradiated strained Fe grains [16].

2.2 Dislocation source cases

In strained Fe grains, cross-slip is a ubiquitous time and stress dependent stochastic mechanism. The effect of cross-slip on dislocation/loop interaction mechanism has recently been evaluated using a specific «composite» dislocation source configuration, representing the dislocation arm arrangement due to a single, well-defined cross-slip event (see Fig. 1(b)). The simulation volume keeps the same crystallographic orientation as before, whereas the dislocation length L_Z = 400 nm ensures sufficient dislocation glide distance, before colliding with the immobile loop. A composite dislocation source of total length L = 300 nm includes two connected arms (or segments): L_{cs} long segment AC gliding in the

cross-slip system; L_p long segment BC gliding in the primary slip system. One facet oriented normal to $[1\bar{1}1]$ or [111] direction with size D = 6 nm is placed at a distance of 15 nm from segment BC. The center of the facet is coplanar with the dislocation line and stands $L_p/2$ off point B. The influence of these simulation parameters have been studied elsewhere (see [15] for details). This work mainly aims at highlighting the loop induced stress field effect, during such dislocation/loop interactions.

Nodes A and B are pinned in all the implemented composite dislocation cases. Node C is common to the two gliding segments and for this reason, has only one degree of freedom, i.e. along the initial dislocation line direction. Once node C contacts node B, the initial dislocation source is entirely transferred into the cross-slip plane and $L_{cs} = L$. It should be noted that non-periodic boundary conditions are used for all pinned configurations and the simulation is terminated whenever a dislocation node reaches one of the simulation volume boundaries or the simulation time achieves the maximal value $t_{max} \sim 10$ ns.

2.3 Activation of the composite dislocation source: theoretical analysis

The total dislocation energy of Fig. 1(b) configuration is the sum of the elastic and core contributions. In the non-singular continuum elastic theory, the elastic energy is given in Appendix Section of [19],[22], whereas the core energy per unit length is [23]:

$$e^{core} = \xi^{core} \frac{\mu b^2}{4\pi(1-\nu)}(1-\nu\cos^2\theta) \tag{3}$$

where $\xi^{core} = 0.257$ is a correction coefficient and θ is the angle between the Burgers vector and the local tangent vector. The correction coefficient and core radius used in the non-singular stress field calculations are calibrated as explained [13],[24]. The total energy of the composite source is thus independent of the cross-slip segment length. In these conditions, there is no driving energy to either shrink or spread the added cross-slip segment, along the initial dislocation source.

In absence of obstacle, segment AC and BC evolutions involve the one-dimensional displacement of the common node C. For segment AC gliding in the cross-slip plane, the core energy contribution to the force exerted on node C can be expressed as:

$$\mathbf{F}^{AC} = e^{core}\mathbf{T} + \frac{de^{core}}{d\theta}\mathbf{N} \tag{4}$$

where **T** and **N** are the corresponding local tangent and normal vectors. Since node C moves parallel to the Burgers vector, projection of this force along the Z-axis yields:

$$F^{AC} = \xi^{core}\frac{\mu b^2}{4\pi(1-\nu)}(1-2\nu+\nu\cos^2\theta_{AC})\cos\theta_{AC} \tag{5}$$

where θ_{AC} is the angle between the Z-axis and the local tangent vector of segment AC at node C. The force from segment BC is given by a similar expression, so the total nodal force corresponds to:

$$F^{C} = \xi^{core}\frac{\mu b^2}{4\pi(1-\nu)}\left[(1-2\nu+\nu\cos^2\theta_{AC})\cos\theta_{AC} - (1-2\nu+\nu\cos^2\theta_{BC})\cos\theta_{BC}\right] \tag{6}$$

A positive force means that the length of segment AC is increasing at the expense of segment BC and vice-versa, for a negative force. Eq. (6) thus indicates that segment AC evolutions are qualitatively the same, regardless of the number of sub-segments (or obstacles) placed beyond node C [25]. In the rest of this work, we therefore focus on the two segments composite sources, for simplicity.

3. Results and discussion

3.1 Benchmarking simulation cases

Fig. 1(a) setup is tested under fixed strain rate loading condition $\dot{\varepsilon}_{YZ} = 10^5$ s^{-1} using a 50 fs time step. This selected loading mode or applied stress tensor minimizes the shear stress acting in the cross-slip system, i.e. one third of the stress acting in the primary slip system [21]. The stress-strain evolutions associated with screw dislocation interactions with $[1\bar{1}1]$, [111] loops and $[1\bar{1}1]$ oriented facets are presented in Fig. 2. In the $[1\bar{1}1]$ loop case, the incoming mobile dislocation breaks away from the loop after releasing a $\boldsymbol{b}$ = [010] dislocation loop. The corresponding dislocation/loop interaction strength is $\Delta\tau_c = 0.4\mu b/(L\text{-}D)$ in good agreement with equivalent MD simulation results [11]. In the [111] loop case, a helical jog is formed along the incoming dislocation line, which then closes itself after the interaction is completed. This reaction is associated with a critical obstacle strength $\Delta\tau_c = 0.72\mu b/(L\text{-}D)$ in agreement with MD predictions (see Fig. 6 of [12]). The loops are then replaced by impenetrable, hard facets. The $[1\bar{1}1]$ facet interaction case corresponds to the Orowan mechanism: the two long dislocation arms reconnect past the hard facet and a loop debris is left behind. The corresponding interaction strength is consistent with Orowan's expression [26]. The result of [111] facet interaction is similar to the former case (not shown). These present results validate the adopted simulation setup and selected material parameters.

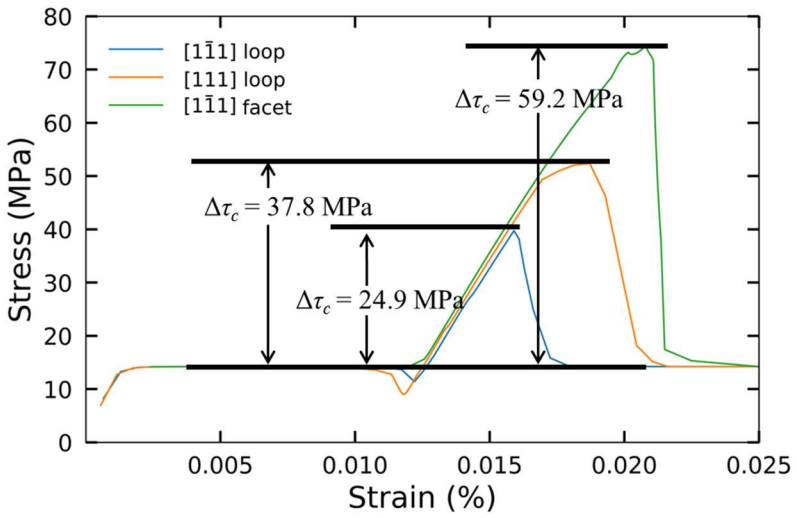

Fig. 2. The stress-strain curves of $[1\bar{1}1]$ loop, [111] loop and $[1\bar{1}1]$ facet benchmarking cases (Fig. 1(a)), respectively.

3.2 Interaction with $[1\bar{1}1]$ *facet*

This section focuses on dislocation interaction with $[1\bar{1}1]$ oriented facet. The coplanar (pinned) dislocation source case with $L = L_p = 300$ nm is carried out under strain-rate controlled conditions. We found that the obstacle strength of $[1\bar{1}1]$ facet is 142 MPa (not shown), which is close to the $[1\bar{1}1]$ loop strength (150 MPa), associated with a similar interaction mechanism. Then the composite dislocation source case is systematically investigated using different (constant) applied stress (τ_p, τ_{cs}) conditions, using finite L_p long dislocation segments gliding in the primary slip plane. Two sets are presented hereafter, in Tab. 2. The selected applied stress magnitudes are comparable to the obstacle strength, in order to ensure that the mobile dislocation moves quickly towards the facet.

	L (nm)	L_p (nm)	$\tau_{p,min}$ (MPa)	$\tau_{p,max}$ (MPa)	$\tau_{p,inc}$ (MPa)	$\tau_{cs,min}$ (MPa)	$\tau_{cs,max}$ (MPa)	$\tau_{cs,inc}$ (MPa)
Set 1	300	300	100	200	20	0	0	20
Set 2	300	150	100	200	20	100	200	20

Tab. 2. Initial simulation sets including a composite dislocation source. Stresses τ_p, τ_{cs} are applied on the primary slip system and cross-slip systems, respectively. Each set corresponds to several different simulations, where (τ_p, τ_{cs}) vary by $\tau_{p,inc}$ and $\tau_{cs,inc}$ 20 MPa stress increments.

Simulation results associated with the Set 2 could be expressed in the form of triplet number series (τ_p, τ_{cs}, S). For instance, S = 0 case indicates that the source is blocked by the obstacle and the S = 2 case indicates that the source overcomes the defect by changing its glide plane, due to cross-slip mechanism.

The corresponding strain rate evolutions are shown in Fig. 3 for τ_p = 120 MPa and different τ_{cs} values ranging from 100 MPa to 180 MPa (curves B, C, D). These results are compared with Set 1 results obtained using L_p = 300 nm (curve A). The strain rate peak visible in curve B indicates the time where the initial source is entirely transferred into the primary slip plane and then, blocked by the interacting facet (as in curve A case); whereas the strain rate peaks in curves C and D indicate the time where the initial source is entirely transferred into the cross-slip plane and thereby, by-passes the facet. The critical interaction stress is clearly affected by the presence of a cross-slipped segment, i.e. $\tau_{critical}(L_p$ = 150 nm) < $\tau_{critical}(L_p$ = 300 nm). Moreover, the strain rate peak time is shifted by about 0.04 ns when compared to the loop case, as compared to Fig. 8(a) of reference [15]. This means the reaction completion time is up to 15% shorter than the actual loop case, depending on the loading conditions.

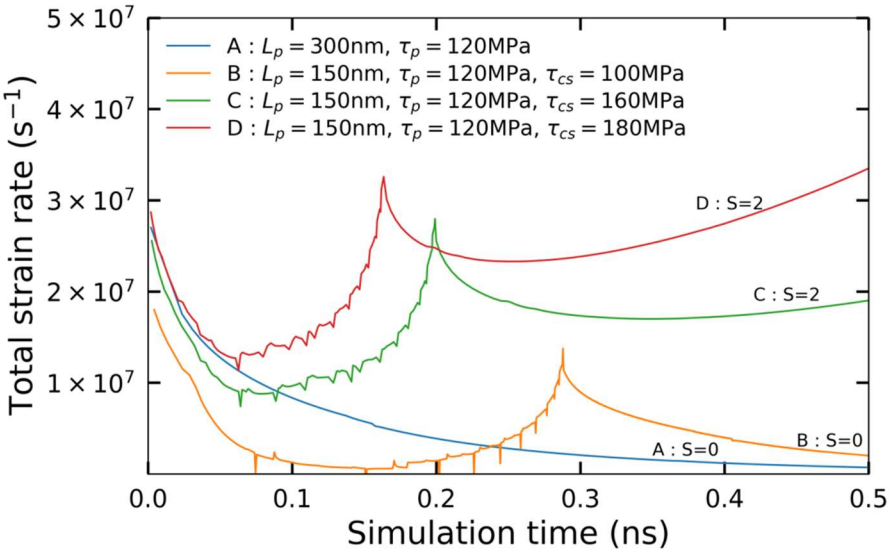

Fig. 3. Total strain rate evolutions versus simulation time associated with simulation setup 2 (L_{cs} = L_p = 150 nm), for different loading combinations (τ_p, τ_{cs}), i.e. τ_p = 120 MPa and τ_{cs} varies from 100 to 180 MPa. The different curves A, B, C, D are further described in the main text.

The total strain and corresponding total strain rate evolutions are shown in Fig. 4 for L_p = 150 nm and loading stresses $\tau_p = \tau_{cs}$ = 120 MPa. These conditions are typically found in a Fe specimen loaded in uniaxial tension, after irradiation up to ~10^{-3} dpa at 300K [5]. In the early stage of the interaction, segment BC glide is aided by the loop-induced stress field, up to marker ①. Node C quickly attains the junction segment formed by segment BC interaction with the loop, in ②. At this point, the local stress field and the junction hinder the continuous movement of node C, which retards the transfer of segment AC towards the cross-slip plane, in ③ and ④. In the facet case for comparison, segment AC displacement is rather continuous, until it is entirely transferred into the cross-slip plane (after ~ 1.2 ns). The reaction time is nearly the same in the loop case (several ps shift), with a relative total strain error of about 3%. Interaction with $[1\bar{1}1]$ loop or facet is thus controlled by the cross-slip mechanism.

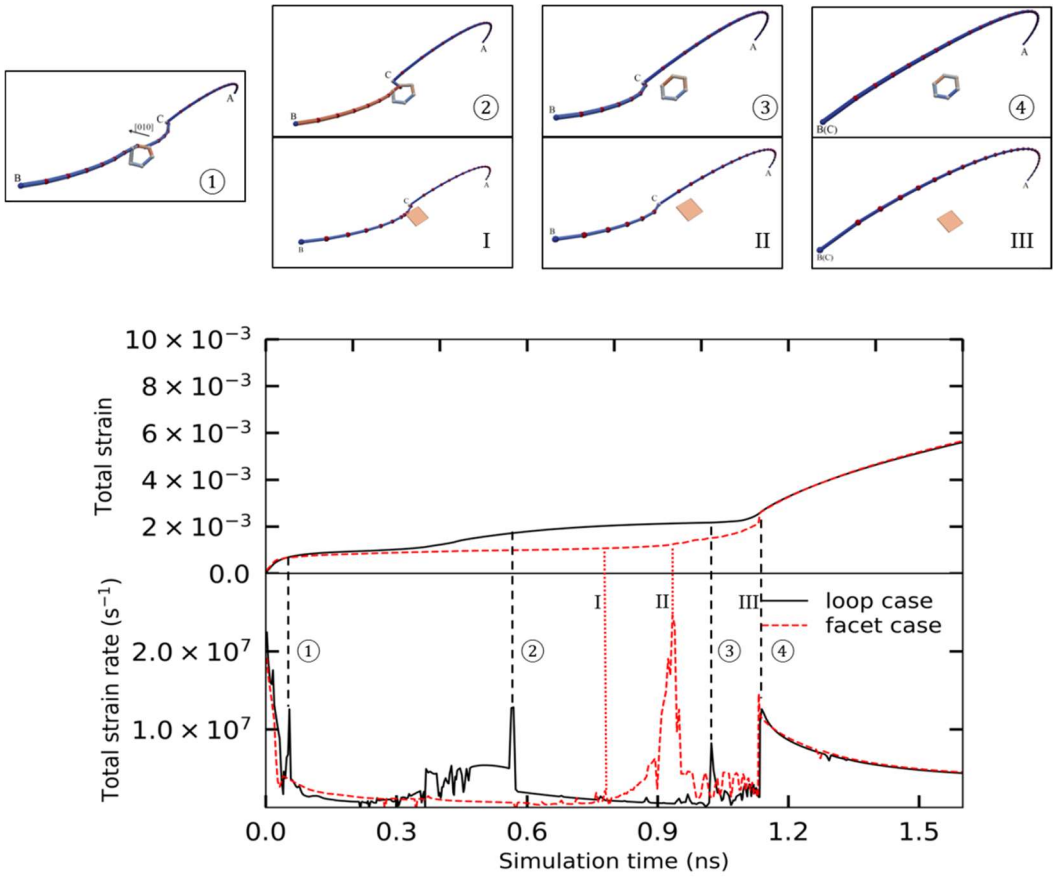

Fig. 4. Total strain (upper frame), total strain rate (lower frame) evolutions and corresponding dislocation configurations. This case corresponds to L_p = 150 nm and loading condition $\tau_p = \tau_{cs}$ = 120 MPa. The loop and facet cases are denoted by solid and dashed lines, respectively. In the loop case, the junction is formed in ①, as the mobile dislocation segment is attracted by the loop; in ②: the common node C approaches the loop; in ③: the dislocation segment unpins from the loop; in ④: the dislocation is entirely transferred into the cross-slip plane. For the facet case, in I: the common node C moves close to the facet; in II: the dislocation segment by-passes the facet; in III: the dislocation is entirely transferred into the cross-slip plane. The small fluctuations taking place between II and III (or ③ and ④) are due to the discrete description of the dislocation segments (node insertion or removal).

3.3 Interaction with [111] *facet*

The [111] facet obstacle strength is 209 MPa, under strain rate controlled loading condition. The different interaction mechanisms associated with the L_p = 150 nm case are presented in Fig. 5, for the applied stress range is comprised between 130 MPa and 280 MPa, in agreement with the prior interaction strength result (since the source can overcome the obstacle in the primary slip system if τ_p > 210 MPa). Compared to the actual loop case, only three different interaction mechanism are here observed (the helical turn formation mechanism is therefore missing). The interaction strength of the composite source is again lower than that in the coplanar source case, under comparable loading conditions.

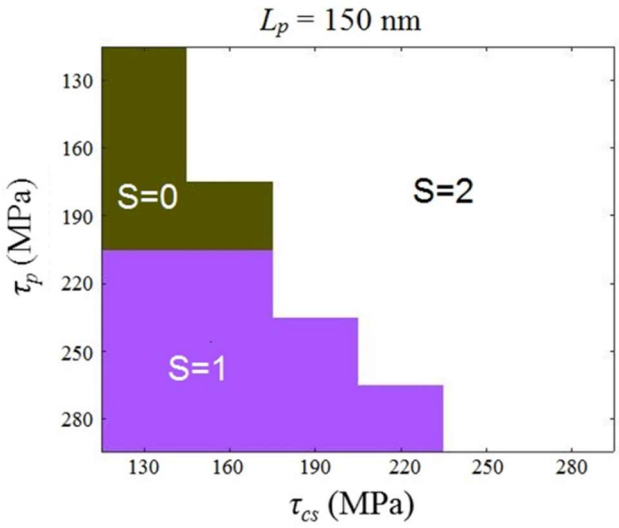

Fig. 5. Composite source interaction (L_p = 150nm) with a [111] facet. The different interaction mechanisms are indicated by different color, depending on the considered applied stress (τ_p, τ_{cs}) combination. S = 0: the source is blocked by the obstacle; S = 1: the dislocation goes through the facet in the primary slip plane; S = 2: the source overcomes the facet while gliding in the cross-slip plane. The present results apply to room temperature straining conditions.

Lastly, interactions with [111] loop and [111] oriented hard facet are compared side to side, in Fig. 6. The interaction curves are much more continuous (flatter) than in Fig. 4 due to the small effective contacting obstacle size, minimizing the number of node insertion operations. It is recalled that unlike in the loop interaction case, the facet case does not generate any stress field and excludes the helical jog formation. The reaction completion time presents a 0.1 ns time shift, between dislocation/loop and dislocation/facet cases. The corresponding relative total strain difference is less than 12%, between the two aforesaid cases.

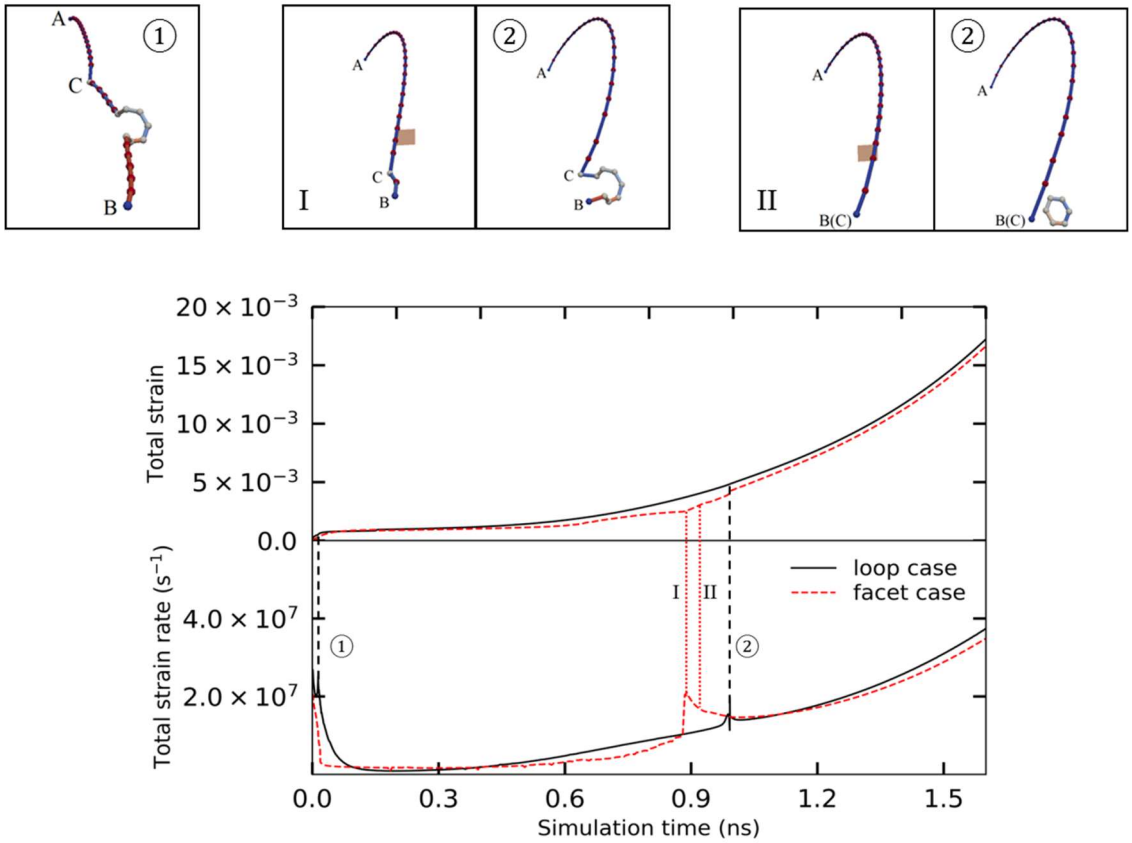

Fig. 6. Total strain (upper frame), total strain rate (lower frame) time evolutions and corresponding dislocation configurations. The represented case corresponds to L_p = 150 nm with loading condition $\tau_p = \tau_{cs}$ = 160 MPa. The loop and facet cases are denoted by solid and dashed lines, respectively. In the loop case, the helical jog is formed in ①, where the mobile dislocation segment is attracted by the loop; in ②: the former helical jog is closed itself and then the dislocation is entirely transferred into the cross-slip plane. In the facet case, in I: the dislocation segment by-passes the facet; in II: the dislocation is entirely transferred into the cross-slip plane.

3.4 General discussion

The loop-induced stress field generally contributes to the dislocation/loop interactions. This contribution can be summarized as follows, based on Section 3.2 and Section 3.3 results:

1. In the presence of cross-slip (composite source), the dislocation/obstacle interaction time is up to 15% longer for a given loop case, with respect to the corresponding facet case. This effect is analogue to adding an extra viscosity, during the whole interaction time. The total reaction time of the [111] facet case with B = 0.14 MPa.ns is indeed identical to that of the [111] oriented loop case (not shown);
2. The total strain shift is up to 12% smaller for a given loop case with respect to the corresponding dislocation/facet case. This effect is mainly ascribed to the actual loop displacement, during the interaction time. In the [111] oriented loop case for example, this corresponds to the formation and propagation of a helical turn. The loop-induced stress field has therefore little effect on stress-strain response associated with the dislocation/loop interaction.

In the composite dislocation source configuration, dislocation/loop interaction mainly depends on node C displacements, which are not significantly affected by the loop-induced stress field, regardless of the interacting loop orientation. Cross-slip is then a major strain rate limiting mechanism, in the investigated case studies.

The critical interaction stress is much weaker in presence of cross-slip, as reported in [27]-[28]. This effect could then explain grain scale plasticity mechanisms [29] and in certain conditions, the corresponding stress-strain response of post-irradiated materials [30]. Dislocation mobility in presence of defect dispersion and cross-slip is accurately described using the proposed, simplified dislocation/facet description. This approach significantly improve the computational efficiency associated with massive (grain scale) DD simulations [21].

4. Conclusions

Interaction between pinned screw dislocation sources and $[1\bar{1}1]$and [111] oriented facets is investigated using 3D nodal dislocation dynamics simulations. A specific «composite» dislocation source including two (L_p, L_{cs}) long segments, gliding in the primary and cross-

slip planes, is examined under various loading combinations (τ_p, τ_{cs}), in terms of interaction mechanisms and time evolution of the strain rate. It is found that the presence of a cross-slipped segment L_{cs} systematically lowers the dislocation/loop and dislocation/facet interaction strengths. These results indicate that cross-slip is possibly the dominant strain rate limiting mechanism during dislocation-mediated straining in presence of loop dispersions.

It is finally shown that screw dislocation mobility in presence of defect dispersions and cross slip can be accurately described using the proposed, facet-loop surrogate approach.

Acknowledgements

This work has been carried out within the framework of the EUROfusion Consortium and has received funding from the Euratom research and training programme 2014-2018 under grant agreement No 633053. The views and opinions expressed herein do not necessarily reflect those of the European Commission. The authors also acknowledge the support of the Materials Research Program RMATE, from the Nuclear Energy Division of the French Atomic Energy Commission (CEA/DEN).

References

[1] M. Matijasevic, W. Van Renterghem, A. Almazouzi, Characterization of irradiated single crystals of Fe and Fe-15Cr, Acta Mater. 57 (2009) 1577-1585.

[2] M. Matijasevic, E. Lucon, A. Almazouzi, Behavior of ferritic/martensitic steels after n-irradiation at 200 and 300°C, J. Nucl. Mater. 377 (2008) 101-108.

[3] K. Farrell, T.S. Byun, N. Hashimoto, Deformation mode maps for tensile deformation of neutron-irradiated structural alloys, J. Nucl. Mater. 335 (2004) 471-486.

[4] D.J. Bacon, F.Gao, Y.N. Osetsky, Computer simulation of displacement cascades and the defects they generate in metals, Nucl. Instrum. Methods. Pyhs. Res., Sect. B 153 (1999) 87.

[5] M. Victorian et al., The microstructure and associated tensile properties of irradiated fcc and bcc metals, J. Nucl. Mater. 276 (2000) 114-122.

[6] Y.A. Nikolaev, A.V. Nikolaeva, Y.I. Shtrombakh, Radiation embrittlement of low-alloy steels, Int. J. Pres. Ves. Pip. 79 (2002) 619-636.

[7] S.J. Zinkle, Y. Matsukawa, Observation and analysis of defect cluster production and interactions with dislocations, J. Nucl. Mater. 329 (2004) 88-96.

[8] B.C. Masters, Dislocation loops in irradiated iron, Phil. Mag. 11 (1965) 881-893.

[9] Q. Wei et al., Evolution and microstructure of shear bands in nanostructured Fe, Appl. Phys. Lett. 81 (2002) 1240-1242.

[10] G.R. Odette et al., Modeling the multiscale mechanics of flow localization-ductility loss in irradiation damaged bcc alloys, J. Nucl. Mater. 307 (2002) 171-178.

[11] X.Y. Liu, S.B. Biner, Molecular dynamics simulations of the interactions between screw dislocations and self-interstitial clusters in body-centered cubic Fe, Scripta Mater. 59 (2008) 51-54.

[12] D. Terentyev, D.J. Bacon, Y.N. Osetsky, Reactions between a ½ <111> screw dislocation and <100> interstitial dislocation loops in alpha-iron modelled at atomic scale, Phil. Mag. 90 (2010) 1019-1033.

[13] X.J. Shi et al., Interaction of <100> dislocation loops with dislocations studied by dislocation dynamics in α-iron, J. Nucl. Mater. 460 (2015) 37-43.

[14] J. Drouet et al., Dislocation dynamics simulations of interactions between gliding dislocations and radiation induced prismatic loops in zirconium, J. Nucl. Mater. 449 (2014) 252-262.

[15] Y. Li et al., Screw dislocation interaction with irradiation defect-loops in α-iron: evaluation of cross-slip effect using dislocation dynamics simulations, Modell. Simul. Mater. Sci. Eng. 26 (2018) 055009.

[16] C. Robertson, E. Meslin, Experimental analysis of the plastic behavior of ion-irradiated bainitic RPV steel, Euratom 7th PCRD, Project PERFORM60, December 2011.

[17] V.I. Alshits, V.L. Indenbom, Mechanisms of dislocation drag, F.R.N. Nabarro Ed., Dislocations in solids, Volume 7, chapter 34, Elsevier, Amsterdam, 1986.

[18] N. Urabe, J. Weertman, Diloscation mobility in potassium and iron single crystals, Mater. Sci. Eng. 18 (1975) 41-49.

[19] W. Cai et al., A non-singular continuum theory of dislocations, J. Mech. Phys. Solids 54 (2006) 561-587.

[20] G. Po et al., A phenomenological dislocation mobility law for bcc metals, Acta Mater. 119 (2016) 123-135.

[21] K. Gururaj, C. Robertson, M. Fivel, Channel formation and multiplication in irradiated FCC metals: a 3D dislocation dynamics investigation, Phil. Mag. 95 (2015) 1368-1389.

[22] V. Bulatov, W. Cai, Computer simulations of dislocations, Vol. 3. Oxford University Press, 2006, Chap. 8.

[23] L. Dupuy, M. Fivel, A study of dislocation junctions in FCC metals by an orientation dependent line tension model, Acta Mater. 50 (2002) 4873-4885.

[24] X.J. Shi, Etude par simulations de dynamique des dislocations des effets d'irradiation sur la ferrite à haute température, Université Pierre et Marie Curie – Paris VI, Ph.D. thesis, 2014, p60.

[25] K. Gururaj, Dislocation dynamics simulations of strain localization in irradiated steels, Homi Bhabha National Institute, Ph.D. thesis, 2013, Chap. 6.

[26] D.J. Bacon, U.F. Kocks and R.O. Scattergood, The effect of dislocation self-interaction on the Orowan stress, Phil. Mag. 28 (1973) 1241-1263.

[27] C.S. Shin et al., Dislocation-impenetrable precipitate interaction: a three-dimensional discrete dislocation dynamics analysis, Phil. Mag. 83 (2003) 3691-3704.

[28] A. Kelly, R.B. Nicholson, Strengthening method in crystals, First ed., Elsevier, New York, 1971, p. 156.

[29] K. Gururaj, C. Robertson, M. Fivel, Post-irradiation plastic deformation in bcc Fe grains investigated by means of 3D dislocation dynamics simulations, J. Nucl. Mater. 459 (2015) 194-204.

[30] Y. Li, C. Robertson, Irradiation defect dispersions and effective dislocation mobility in strained ferritic grains: A statistical analysis based on 3D dislocation dynamics simulations, J. Nucl. Mater. 504 (2018) 84-93.